Available online at www.sciencedirect.com
ScienceDirect
Journal of the European Ceramic Society 32 (2012) 97–105
www.elsevier.com/locate/jeurceramsoc

TaB_2-based ceramics: Microstructure, mechanical properties and oxidation resistance

Laura Silvestroni *, Stefano Guicciardi, Cesare Melandri, Diletta Sciti

CNR-ISTEC, Institute of Science and Technology for Ceramics, Via Granarolo 64, I-48018 Faenza, Italy

Received 24 March 2011; received in revised form 14 July 2011; accepted 23 July 2011
Available online 19 August 2011

Abstract

TaB_2-based ceramics were hot pressed in low vacuum with addition of 5–10 vol% $MoSi_2$. Temperatures in the range of 1680–1780 °C led to relative density around 90–95%. The hardness was about 18 GPa, the fracture toughness 4.6 MPa $m^{1/2}$ and the room temperature flexural strength was around 630 MPa, but abruptly decreased above 1200 °C to 220 MPa. The composite containing 10 vol% of $MoSi_2$ was tested in a bottom-up furnace in the temperature range 1200–1700 °C for 30 min. The microstructure appeared covered by a SiO_2 layer, whose thickness increased with the temperature, but the bulk remained unaltered up to 1600 °C. At 1700 °C the specimen vaporized. Nanoindentation was employed on the oxidized cross sections in order to detect eventual mechanical properties modification associated to chemical/microstructural change, like formation of Ta–B–O solid solutions.

Keywords: TaB_2; Microstructure; Mechanical properties; Oxidation resistance; Nanoindentation

1. Introduction

Transition metal borides are widely recognized as an attractive class of materials for a broad range of mechanical applications in abrasive, erosive, corrosive and high-temperature environments, owing to their high melting points and hardness, thermodynamic stability and excellent electrical conductivity. To date, most studies have focused on the borides of Ti, Zr and Hf for application as cutting tools, for molten metals processing or as sharp components of new generation space vehicles in ultra-high temperature environments.[1–3] Tantalum diboride possesses good corrosion resistance, chemical stability, high melting point, good hardness and high heat conductivity. The addition of TaB_2 to other matrices has been studied in the past years. Talmy et al.[4] found that the oxidation resistance of ZrB_2–SiC materials was significantly improved when ZrB_2 was partially replaced by TaB_2. More specifically, when comparing the effect of the addition of 10 mol% of various metal diborides, i.e. TiB_2, NbB_2, VB_2, CrB_2, and TaB_2, the latter one was found to guarantee the highest protection to the modified ZrB_2–SiC ceramic when exposed to air at 1300 °C for 5 h.[4] More recently, the study of the influence of the TaB_2 content on the oxidation resistance of ZrB_2-based ceramics received renewed attention.[5–7] It has been proved that tantalum additions to ZrB_2–B_4C–SiC in the form of TaB_2 and/or $TaSi_2$ increases the oxidation resistance over the temperature range 1150–1550 °C, $TaSi_2$ being the most effective one.[5] The improvement in the oxidation resistance of the ceramic composite as a consequence of the addition of TaB_2 beyond 3.32 mol% was confirmed at 1200 and 1400 °C, while this property worsens at 1500 °C. Moreover, the beneficial influence of tantalum diboride on the oxidation resistance, densification behavior and mechanical properties of TaC–10 wt% TaB_2, as compared to monolithic TaC, was also demonstrated.[8]

Very few are the studies focused on the characterization of massive TaB_2-ceramics. Zhang et al. investigated the microstructure and the mechanical properties of a TaB_2 ceramic obtained after hot pressing at 2000 °C of synthesized powder.[9] Recently, Licheri et al.[10] obtained a 96% dense TaB_2–SiC material after spark plasma sintering of mechanically activated Ta, B_4C and Si reactants at 1800 °C for 30 min.

The oxidation behavior of TaB_2 powder was studied at 1000 °C for 25 h by Matsushita et al.,[11] but concerning bulk ceramics, the oxidation behavior of TaB_2 has not been studied as extensively as other transition metal diborides such as ZrB_2

* Corresponding author. Tel.: +39 0546 699723; fax: +39 0546 46381.
E-mail address: laura.silvestroni@istec.cnr.it (L. Silvestroni).

0955-2219/$ – see front matter © 2011 Elsevier Ltd. All rights reserved.
doi:10.1016/j.jeurceramsoc.2011.07.032

and HfB_2.[12] On the other hand, studies on tantalum oxidation in the range 1000–1800 °C at different oxygen partial pressures, were performed in the 60s by Kofstad.[13,14]

In the present study, tantalum diboride was hot pressed to high density with the addition of 5–10 vol% of $MoSi_2$. Mechanical properties, such as hardness, fracture toughness, Young's modulus and flexural strength from room temperature to 1500 °C in air, were measured and compared to other TaB_2-based composites available in the literature. Finally, the oxidation behavior in a bottom-up furnace from 1200 to 1700 °C was studied and correlated to nanoindentation measurements.

2. Experimental procedure

Commercial powders were used to prepare the ceramic composites: hexagonal TaB_2 (Cerac Inc., Milwaukee, WI), purity 99.5%, −325 mesh, particle size range 5–10 μm; tetragonal $MoSi_2$ (<2 μm, Aldrich, Steinbeim, Germany), particle size range 0.3–5 μm and oxygen content ∼1 wt%. Mixtures with 5 and 10 vol% of $MoSi_2$ were prepared, TBM5 and TBM10, respectively.

The powder mixtures were ball milled for 24 h in absolute ethanol using silicon carbide milling media. Subsequently the powders were dried in a rotary evaporator and sieved through a 60-mesh screen. Hot-pressing was conducted in low vacuum (∼100 Pa) using an induction-heated graphite die with a constant uniaxial pressure of 30 MPa, a heating rate of 20 °C/min and free cooling. For each composition, the maximum sintering temperature was set on the basis of the shrinkage curve. The bulk densities were measured by Archimedes' method. Crystalline phases were identified by X-ray diffraction (Siemens D500, Germany). The microstructure was analysed using scanning electron microscopy (SEM, Cambridge S360, Cambridge, UK) and energy dispersive spectroscopy (EDS, INCA Energy 300, Oxford instruments, UK) on fractured and polished surfaces. Mean grain size, amount of porosity and secondary phases were determined through image analysis on SEM micrographs of polished surfaces using a commercial software program (Image Pro-plus 4.5.1, Media Cybernetics, Silver Springs, MD, USA). At least 100 grains per specimen were measured for the determination of the mean grain size. TEM samples were prepared by cutting 3 mm discs from the sintered pellets. These were mechanically ground down to about 80 μm, created a dimple to about 10 μm and then further ion beam thinned until small perforations were observed by optical microscopy. Transmission Electron Microscope analysis was performed by a FEI Tecnai F20 ST, with an acceleration voltage of 200 kV, equipped with an EDAX EDS X-ray spectrometer PV9761 with Super Ultra thin window.

Vickers microhardness (HV1.0) was measured with a load of 9.81 N using a Zwick 3212 tester. Young's modulus (E) was measured by the resonance frequency method on 28 mm × 8 mm × 0.8 mm specimens using a HP gain-phase analyzer. Fracture toughness (K_{Ic}) was evaluated using chevron-notched beams (CNB) in flexure. The test bars, 25 mm × 2 mm × 2.5 mm (length by width by thickness, respectively), were notched with a 0.1 mm-thick diamond saw; the chevron-notch tip depth and average side length were about 0.12 and 0.80 of the bar thickness, respectively. The specimens were fractured using a semi-articulated silicon carbide four-point fixture with a lower span of 20 mm and an upper span of 10 mm using a screw-driven load frame (Instron mod. 6025). The specimens, three for each composite, were loaded with a crosshead speed of 0.05 mm/min. The "slice model" equation of Munz et al.[15] was used to calculate K_{Ic}. On the same machine and with the same fixture, the flexural strength (σ) was measured at room temperature, 1200 °C and 1500 °C in air on chamfered bars 25 mm × 2.5 mm × 2 mm (length × width × thickness, respectively), using a crosshead speed of 0.5 mm/min. Before the bending test, a soaking time of 18 min was set to reach thermal equilibrium. For the best composition, 5 specimens were tested at room temperature and 3 at high temperature.

The oxidation resistance was tested at 1200, 1500 and 1600 °C on 13 mm × 2.5 mm × 2 mm bars in static air in a bottom-up loading furnace box (Nannetti FC/18, Faenza, Italy). The specimens were located in the furnace on ZrO_2 supports when the maximum temperature was reached and then removed and air quenched after an exposure time of 30 min. All the specimens were previously cleaned in acetone. The mass of the specimens was measured before and after exposure. The microstructural modifications induced in the oxidized specimens were evaluated by XRD and SEM-EDS on surface and cross section.

In order to detect any variation induced by oxidation on mechanical properties, nanoindentation tests were carried out on the polished cross sections of the oxidized bars using a commercial nanoindenter (Nano Indenter XP™, MTS Systems Corporation, Oak Ridge, TN, USA) fitted with a Berkovich diamond tip. The indentations were performed across a thickness of about 1 mm starting right underneath the silica layer toward the core of the bar with a constant step of 15 μm up to 60 μm, then at 600 μm and finally at 1 mm. A peak load of 5 mN was used to investigate nanohardness and indentation modulus and at least 40 indentations were made for each position. The indenter was continuously loaded up to the peak load in 15 s and immediately unloaded with no holding time. Nanohardness and indentation modulus were calculated by the data acquisition software of the nanoindenter (TestWorks™ ver. 4.06A), which is based on the model of Oliver and Pharr.[16] The software automatically corrected the raw load–displacement data for the machine compliance and thermal drift. Before the tests, the area function of the indenter tip was calibrated on a standard fused silica specimen.

3. Results and discussion

3.1. Densification behavior

Independent of the sintering additive content, 5 or 10 vol%, the shrinkage started at around 1530 °C, but the maximum temperature required to achieve the maximum shrinkage was 1780 °C for TaBM5 and 1680 °C for TaBM10, respectively, confirming the beneficial effect of $MoSi_2$ during densification.

The relative densities, determined as the ratio between bulk and theoretical densities calculated on the basis of starting compositions were below 90% for both the composites, Table 1. However, as SEM analyses ascertained the presence of a notable amount of extra low-density phases such as SiC and SiO_2, these values might be underestimated, as discussed in the next paragraph.

3.2. Microstructure

The X-ray diffraction pattern in the upper part of Fig. 1 shows the spectrum of TBM10 after sintering: hexagonal TaB_2 and traces of $MoSi_2$ and quartz (2θ=26°) are present. The TaB_2 lattice parameters are the same as those reported in the PDF card #65-1462, no evidence of cell shrinkage can be observed, in contrast to other hexagonal transition metals borides containing $MoSi_2$ or $TaSi_2$, which show satellite peaks with reduced lattice parameters belonging to a $(M,Mo)B_2$ solid solution.[17,18] Indeed, the atomic radius of tantalum and molybdenum are very close, 1.43 and 1.36 Å, respectively; hence, even if Mo substituted in Ta sites in the TaB_2 lattice, it would be very difficult to detect a peak shift by this technique.

The fracture section of TBM5 was intergranular and the matrix grains were not well bonded, as discrete residual porosity was still present and necks were at the early stage of formation. Despite being sintered at 100 °C less, the composite TBM10 had a denser microstructure compared to TBM5 and a good adhesion was found between matrix and secondary phase. The TaB_2 mean grain size was around 3–4 μm for both the composites. The polished surface of TBM10 (Fig. 2a) shows a multi-phase microstructure, the bright phase is TaB_2, the grey phase is $MoSi_2$, while the dark phase is SiO_2 and Si–O–C. Oxygen contaminations derive from impurities in the starting powders and further oxygen take up can derive from exposure to air and the milling procedure. About 8 vol% of silica pockets and SiC particles was calculated by image analysis and the final relative density increased to 95% for TBM10, which is more consistent with the low amount of porosity observed by SEM analysis. SiO_2 contamination was already observed in other composites containing $MoSi_2$ as secondary phase.[19] Its presence in the final microstructure is related to the low sintering temperature, 1680 °C, compared to other Zr- and Hf-borides (1750 and 1900 °C, respectively), which prevented carbo-reduction.[20,21] Large agglomerates of SiC were also occasionally detected, standing adjacent to silica-based phases. At the triple junctions, dark regions containing Ta–Si–B–O and Ta–Si–C–O were observed and intergranular films could also be noticed, as illustrated in Fig. 2b. Inside $MoSi_2$ phase, Si–C–O based products were often noticed (Fig. 2c). Besides, a (Mo,Ta)B phase was observed with white contrast and low dihedral angles. A thorough SEM analysis evidenced a slight contrast inside the matrix grains (Fig. 2d), but the EDS did not clearly reveal a chemical composition difference between the inner and the outer region of the grains, as observed for other transition metal diborides.[17]

By TEM-EDS analysis additional features were identified, as follows. Mo peak was detected all across the TaB_2 grains, indicating the nominal TaB_2 grain are instead a continuous

Table 1
Compositions, sintering parameters, mean grain size and mechanical properties of the TaB_2-based composites. Fracture toughness measurement technique: CNB – chevron-notched beam, ISB – indentation strength in bending, DCM – direct crack measurement.

Composition (vol%)	Sintering (°C/min/MPa)	ρ (g/cm³)	Rel. ρ (%)	M.g.s. (μm)	HV (GPa)	E (GPa)	K_{Ic} (MPa m$^{1/2}$)	σRT (MPa)	σ1200 (MPa)	σ1500 (MPa)	Ref.
TaB_2 + 5 $MoSi_2$	1780/8/30	10.99	90, 91[a]	4	–	–	–	–	–	–	Present study
TaB_2 + 10 $MoSi_2$	1680/8/30	10.78	89, 95[a]	3.5	18.1 ± 0.8	535 ± 4	4.55 ± 0.08 CNB	626 ± 11	219 ± 20	114 ± 5	Present study
TaB_2	2000/45/30	–	98%	3.5–5	25.6 ± 0.7[b]	551 ± 8	4.5 ± 0.3 ISB	555 ± 103			9
TaB_2 + 30 SiC	1800/30/20	–	96%	4	18.9 ± 0.4	–	8.4 ± 0.8 DCM				10
TaB_2 + 25 SiC	1900/60/32		98.6	20	19.1 ± 0.4[c]	468	3.35 ± 0.38 DCM	608 ± 64	–	–	12

[a] Including SiO_2.
[b] 5 kg.
[c] 2 kg.

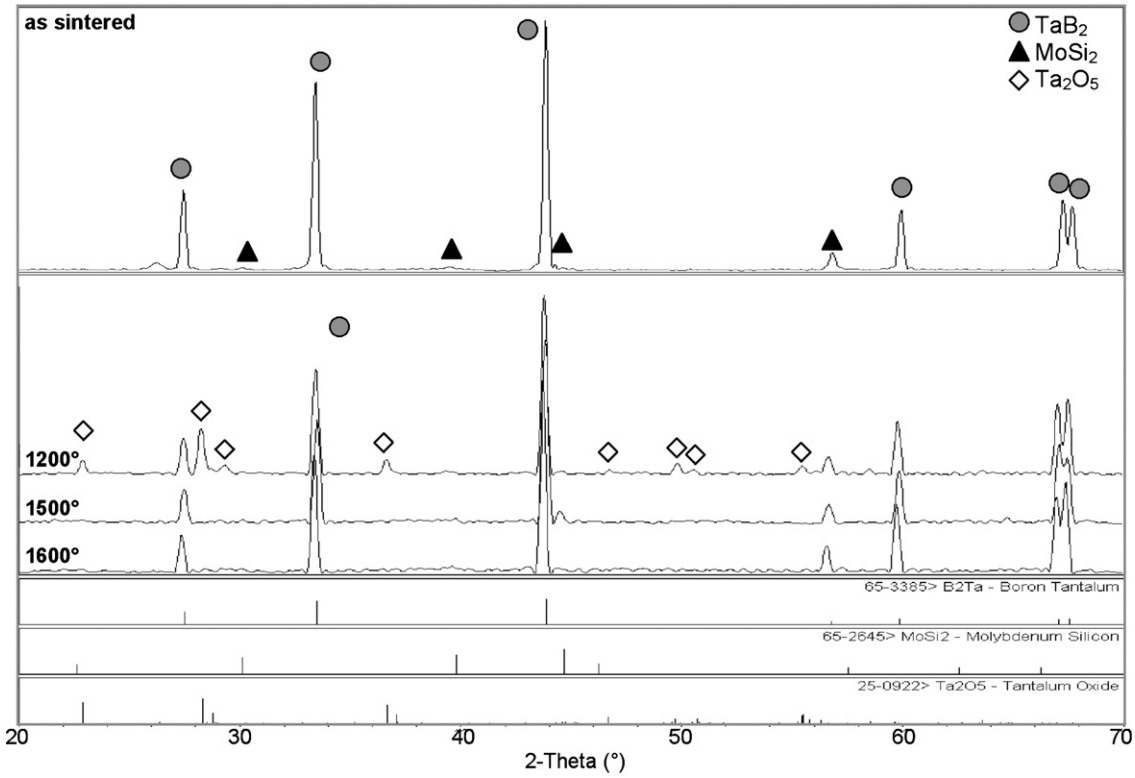

Fig. 1. X-ray diffraction spectra of TaBM10 as sintered and after the oxidation tests.

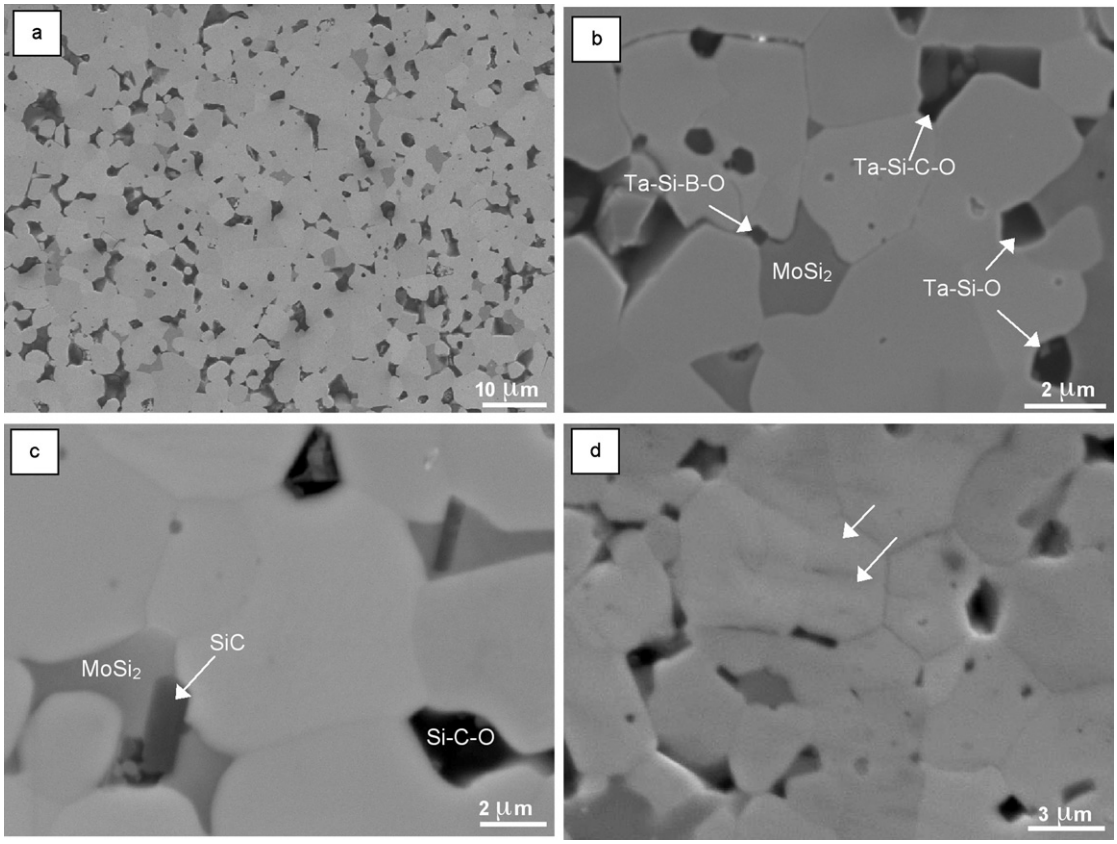

Fig. 2. Polished section of TBM10 showing (a) the overall microstructure, (b and c) the secondary phases and (d) contrasts in TaB_2 grains suggesting a different chemical composition between inner and outer region as indicated by arrows.

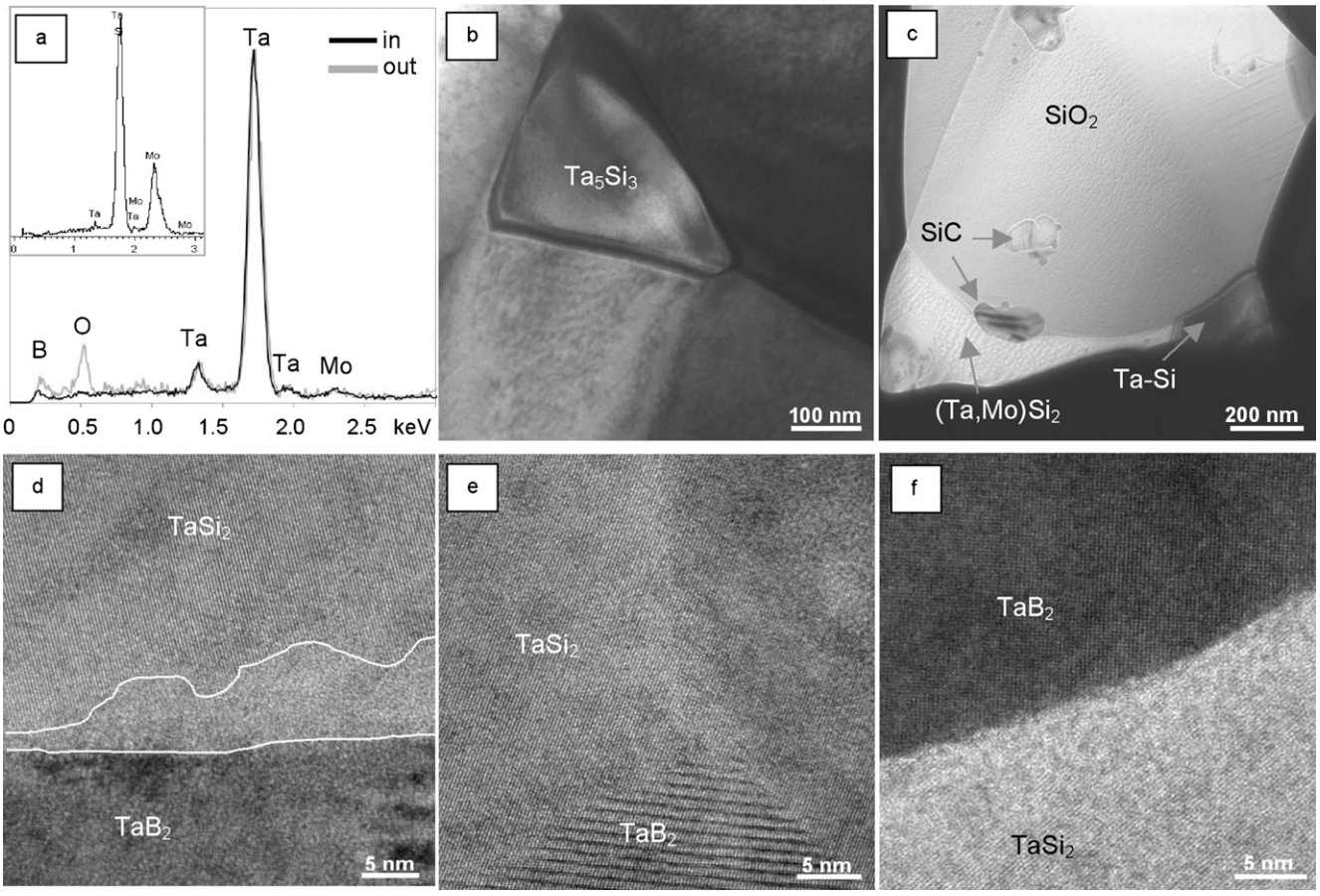

Fig. 3. (a) EDS spectra recorded during TEM session on the inner and outer region of a TaB_2 grain and $MoSi_2$ spectrum in the inset. BF-TEM images showing (b) the Ta_5Si_3 phase at the triple point junction and (c) a SiO_2 pocket containing SiC particles and surrounded by Ta- and Mo-silicides. HR-TEM images showing (d) wetted and (e and f) non wetted interfaces between TaB_2 and $TaSi_2$.

$(Ta,Mo)B_2$ solid solution containing around 5 at% of Mo. The spectra in Fig. 3a were recorded on the inner and outer region of a TaB_2 grain and confirmed that the only compositional difference was the presence of oxygen in the outer region. $MoSi_2$ phase always contained tantalum traces (inset in Fig. 3a) and Ta_5Si_3 or $TaSi_2$ were found at the triple points (Fig. 3b). Nano-sized SiC crystals were identified inside SiO_2 pockets, adjacent to $(Mo,Ta)Si_2$ (Fig. 3c).

High resolution TEM studies revealed both wetted (Fig. 3d) and non-wetted interfaces between TaB_2 and the newly formed $TaSi_2$ (Fig. 3f). The amorphous phase in Fig. 3d contained Ta, Si, B and O. No Mo was recorded in the residual grain boundary phases and spurious Ta–Si–B–O phases had a higher wettability than Ta–Si–O, as the former formed intergranular films while the latter formed isolated pockets.

The comparison with previously studied zirconium and hafnium boride materials sintered with $MoSi_2$, suggests that densification is activated by alike mechanisms. The most important function of $MoSi_2$ is the removal of oxygen bearing species from the surface of TaB_2 particles, generally recognized as the main obstacles for densification, i.e. B_2O_3 and Ta_2O_5. Probable reactions are thus:

$$Ta_2O_5 + MoSi_2 \rightarrow (Ta–Si–O)_{liquid} + (Mo, Ta)_5Si_3 \quad (1)$$

$$B_2O_3 + MoSi_2 \rightarrow (Si–B–O)_{liquid} + Mo \quad (2)$$

These reactions lead to $MoSi_2$ consumption, formation of silica-based liquid phases and Ta/Mo-rich species, such as $(Mo,Ta)_5Si_3$. The silica-based liquids possessed a good wettability toward the boride, promoting dissolution, diffusion and re-precipitation. Through the liquid, diffusion of Mo cations deriving from reaction (2) occurred, leading to formation of $(Ta,Mo)B_2$ and (Ta,Mo)B solid solutions.

$$TaB_2 + Mo = (Ta, Mo)B_2 \quad (3)$$

During re-precipitation, an oxygen-rich layer formed in the proximity of the TaB_2 grain boundary and small particles of $TaSi_2$ or Ta_5Si_3 precipitated from the liquid phase in the vicinity of SiO_2-based pockets.

A possible path for the above mentioned reactions is sketched in Fig. 4. Other concurrent phenomena were the carburization of SiO-based phases, leading to formation of SiC particles inside the liquid phase. This is a consequence of the carbo-thermal reducing environment in which the sintering took place.

3.3. Mechanical properties

Values for mechanical properties are summarized in Table 1 together with some data available from literature for other TaB_2-

Table 2
Compositions, sintering parameters and mechanical properties of some transition metal diborides hot pressed with addition of $MoSi_2$. HV = micro hardness 1 kg, E = Young's modulus, K_{Ic} = fracture toughness, σ = 4-pt flexural strength.

Composition (vol%)	Sintering (°C/min/MPa)	HV (GPa)	E(GPa)	K_{Ic}(MPa m$^{1/2}$)	σRT(MPa)	σ1200(MPa)	σ1500(MPa)	Ref.
TaB_2 + 10 $MoSi_2$	1680/8/30	18.1 ± 0.8	535 ± 4	4.55 ± 0.08	626 ± 11	219 ± 20	114 ± 5	Present study
ZrB_2 + 15 $MoSi_2$	1750/20/30	14.9 ± 0.5	–	3.50 ± 0.60	704 ± 98	–	333 ± 31	[19]
HfB_2 + 15 $MoSi_2$	1900/10/30	20.6 ± 0.4	530	3.82 ± 0.05	742 ± 151	664 ± 28	548 ± 26	[20]

based materials. The mechanical properties were measured only for the composite containing 10 vol% of $MoSi_2$, due to the poor density of TBM5.

The Vickers hardness of the composite was ~18 GPa, which is in the same range of the values reported for other TaB_2-based composites.[9,10,12,22] Also the value of Young's modulus, 535 GPa, compares well to the 551 GPa reported for a pure TaB_2 material prepared by Zhang et al.[9] and it is higher than TaB_2–SiC produced by reactive hot pressing by Lee.[12] The room-temperature strength, 630 MPa, was associated with a very small standard deviation, which is an indication of a homogeneous microstructure. The strength value dropped to 220 MPa at 1200 °C and to 115 MPa at 1500 °C. The load-displacement curves were linear up to 1200 °C, but strongly nonlinear at 1500 °C, owing to the softening of the silica phase.

Table 2 compares the typical sintering temperatures and the mechanical properties for the present TaB_2–10 vol% $MoSi_2$ material with other borides processed with $MoSi_2$, i.e. ZrB_2 and HfB_2.[20,21]

It is worth noting that ZrB_2 and HfB_2 needed a much higher densification temperature than TaB_2, HfB_2 being the most refractory among the three systems. On the other hand, the presence of SiO_2-based residual phases is very limited in the latter, due to retarded pore closure that allowed silica elimination via carbo-reduction.[21] Silica residuals were relatively more abundant in Zr-borides, but still much lower than in TaB_2.

The presence of higher amount of silica-based liquid phase allowed densification to occur at relatively lower temperatures compared to Hf or Zr-borides. However, as a drawback, the mechanical properties were significantly affected by the presence of these secondary phases. In particular, the high-temperature strength of TaB_2 was significantly lower than HfB_2 (550 MPa) and ZrB_2 (330 MPa).

It is very likely that adjusting the powder processing and sintering cycle could reduce the high amount of SiO_2 present in the microstructure and higher values of mechanical properties could be achieved both at room and high temperature.

3.4. Oxidation behavior

A photo of the specimens before and after the oxidation at 1200, 1500, 1600 and 1650 °C is shown in Fig. 5a. This picture clearly evidences that the color of the surface did not undergo appreciable change until 1600 °C. Accordingly, volume and mass change were not significant. The last bar on the right of Fig. 5a resulted from the oxidation at 1650 °C, the white ceramic underneath the bar phase is part of the ZrO_2 support,

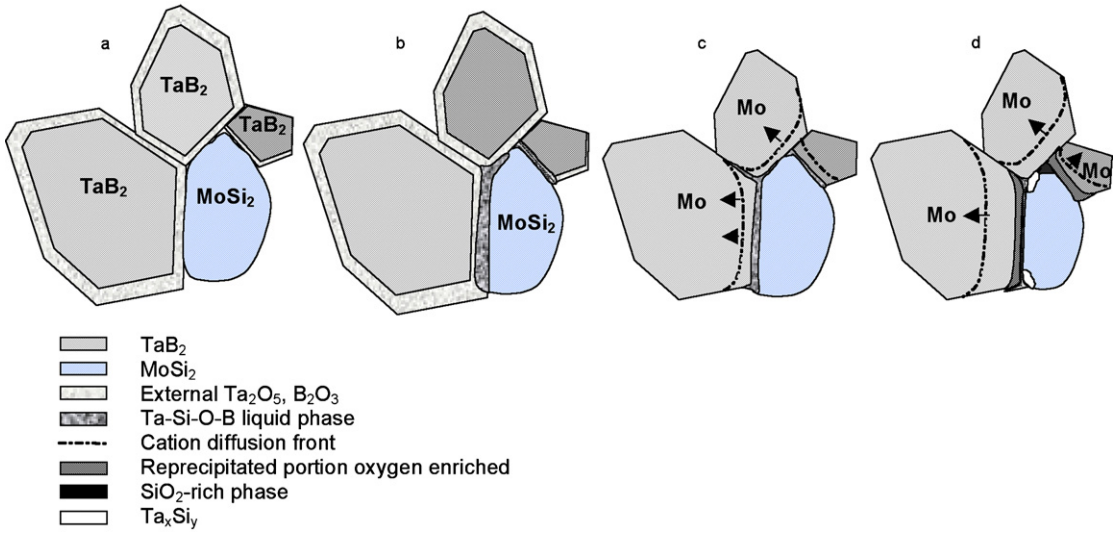

Fig. 4. (a) Initial configuration, TaB_2 particles in contact with $MoSi_2$ additive, (b) reaction between external oxide layer and $MoSi_2$ phase and initial formation of liquid Si–O–Ta–B phase, (c) removal of oxide external layer from TaB_2 particle, densification and interdiffusion of Ta and Mo cations, (d) reprecipitation of solid species from liquid phase, continuous movement of the Mo and Ta diffusion front, formation of discrete silica pockets and Ta_xSi_y precipitates.

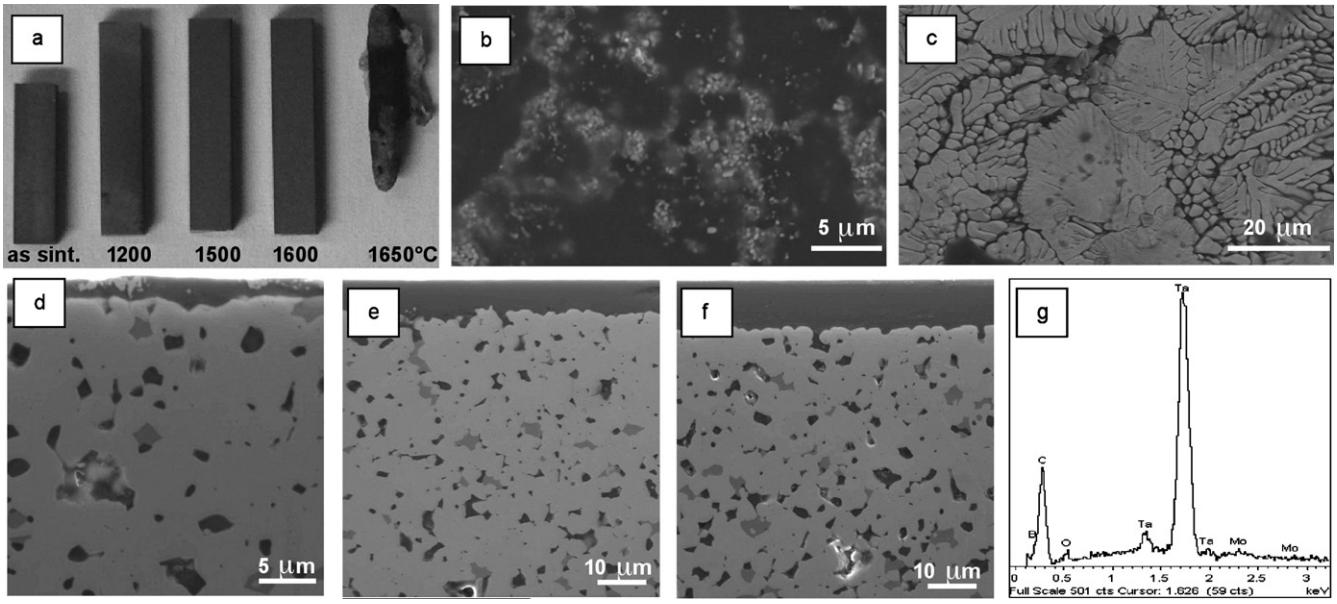

Fig. 5. (a) Appearance of the bars before and after oxidation at 1200, 1500, 1600 and 1650 °C. (b) Ta_2O_5 crystals dispersed in silica-glassy layer on the oxidized surface at 1200 and (c) external surface of the bar oxidized at 1650 °C. Polished cross section of the specimen which underwent oxidation at (d) 1200, (e) 1500 and (f) 1600 °C and (g) EDS spectrum of a typical TaB_2 grain at 60 μm underneath the silica layer.

which could not be totally detached from the sample, due to the interaction with silica. During oxidation test at 1700 °C the sample completely vaporized inside the furnace.

The X-ray diffraction patterns of the oxidized bars at 1200, 1500 and 1600 °C are reported in the bottom part of Fig. 1. At 1200 °C TaB_2 and Ta_2O_5 were detected on the surface. At 1500 °C the oxide peaks were no more visible and only the TaB_2 peaks were present. At 1600 °C the X-ray spectra was very similar to that at 1500 °C. The reason why tantalum oxide was not detected after treatment at 1500 and 1600 °C could be its fast evaporation at 1550 ± 30 °C.[23] No TaB_2 lattice expansion could be detected, however oxygen enrichment and dissolution in TaB_2 cell cannot be ruled out, for analogy to other studies on tantalum oxidation.[13]

SEM observations on the surfaces were consistent with the X-ray diffraction findings. At 1200 °C Ta_2O_5 crystals were embedded into SiO_2 glassy layer (Fig. 5b), but at higher temperatures the surface appeared as a continuous glassy layer. In Fig. 5c the surface of the sample oxidized at 1650 °C is shown. The surface appears like Ta_2O_5 crystals in a leaf shape, no trace of silica-based species is present, the structure is very jagged and open to oxygen penetration. The formation of Ta_2O_5 was so violent and accompanied by a large volume increase, around 60% from TaB_2 to Ta_2O_5, that complete opening of the sample occurred leaving all the other species exposed to direct oxidation. The generated oxide layer provided sufficient room to accommodate all the silica formed upon $MoSi_2$ oxidation. Therefore, no continuous silica layer was found on the surface.

The fast evaporation of tantalum oxide was already reported by Kofstad.[13,14] What happened might also suggest that above 1600 °C, dissociation of tantalum oxide occurred developing α-Ta and liquid phase with high vapor pressure.[23] This experiment marked the limit temperature of 1600 °C that TaB_2-composites can successfully bear in a static oxidizing environment.The cross sections of the oxidized specimen were polished and analysed by SEM. The only differences among them was the SiO_2 layer thickness, which passed from 2.5 to 6 and 9 μm with increasing temperature, 1200, 1500 and 1600 °C, and the presence of Ta–O crystal in the glassy layer at 1200 °C (Fig. 5d–f). It is important to underline that at all the temperatures, in TaB_2 grains down to 60 μm, oxygen peak was detected by EDS (Fig. 5g), suggesting the possibility that oxygen entered in solid solution with the boride. The same was true for the $MoSi_2$ phase, but no oxidation products such as Mo_5Si_3 or MoB were observed below the silica layer. These features may suggest that the small traces of tantalum dissolved in the external glassy scale increased the viscosity of the silico-boride layer and constituted an effective barrier against oxygen penetration.[5–7]

Possible reaction taking place up to 1600 °C are thus:

$$TaB_2 + O_2 = Ta\text{–}B\text{–}O_{ss} \quad (4)$$

$$2TaB_2 + 11/2O_2 = Ta_2O_5 + 2B_2O_3 \quad (5)$$

$$MoSi_2 + 7/2O_2 = 2SiO_2 + MoO_3 \quad (6)$$

While above 1600 °C, the vaporization of tantalum oxide is the dominant phenomenon.

Nanoindentation measurements, performed on the cross section of the bars oxidized at 1200 °C and 1600 °C, are shown in Fig. 6. In the first 60 μm under the SiO_2 layer (inset in Fig. 6a), the analysis did not show evidence of any significant difference in nanohardness, either as a function of position across the specimen, or of the oxidizing temperature, thus suggesting that the TaB_2 grains oxidized at 1200 °C and 1600 °C share the same chemistry without any significant lattice distortion at this depth. A significant hardness increase, from about 23 GPa to

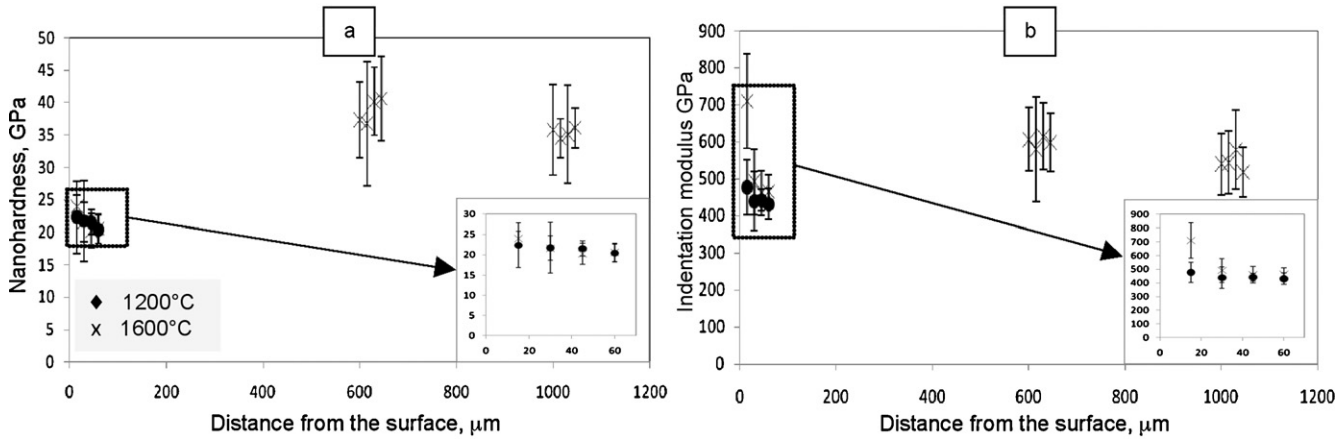

Fig. 6. Nanoindentation results showing (a) nanohardness and (b) indentation modulus as a function of the position below the SiO_2 layer and oxidizing temperature. Each point is the mean of 40 values. Bars represent ±1 standard deviation. In the insets, the expansion of the data indicated by the rectangle.

about 38 GPa, was instead observed at 600 μm and confirmed at 1 mm down to the bulk. The oxidized layer with low value of nanohardness, from the chemical point of view, is characterized by the presence of SiO_2 pockets and oxygen incorporation in TaB_2 grains which formed the Ta–B–O solid solution. Both these factors promoted a hardness decrease due to the low hardness of SiO_2, the grain boundary silicates and the lattice distortion with creation of defects generated by the oxygen diffusion.[13] Below this oxidized layer, SiO_2 and oxygen content decreased moving toward the bulk and the nanohardness attained a more typical value of the TaB_2 phase. The higher value of nanohardness compared to the Vickers hardness can be explained on the basis of the well-known indentation size effect (ISE).[24]

The indentation modulus values in the first 60 μm under the surface are shown in the inset of Fig. 6b. Most of the values showed no difference with position or oxidizing temperature. The only value significantly different from the others is that measured at 15 μm below the surface for sample oxidized at 1600 °C. At the moment, there is no clear explanation for such a high value and further analyses are in progress to confirm this datum. Moving toward the bulk of the samples, the indentation modulus passed from about 480 GPa to about 560 GPa at 1 mm, showing the same trend as the nanohardness. Again, the presence of SiO_2 pockets and diffusional oxygen in regions close to the surface can explain this behavior. The values of indentation modulus compares well to the value of Young's modulus measured by resonant frequency.

The oxidation phenomena extensively studied and modeled for TiB_2, ZrB_2 and HfB_2 with addition of Si-bearing species, as SiC or $MoSi_2$,[25–27] seem not to be valid for TaB_2 when the oxidation temperature is in excess of 1600 °C. At higher temperatures the oxidation process is chiefly affected by extensive formation of Ta_2O_5 accompanied by large volume expansion and its vaporization together with silica-based species.

Dealing with tantalum-based compounds, it can be said that they are extremely stable until a threshold temperature, after which very fast decomposition occurs. On one hand, this aspect is positive because no appreciable bulk modification occurs, but it can become extremely wasting if the limit temperature of 1600 °C is exceeded. This feature needs to be underlined in view of potential applications, because the absence of a steady intermediate state can result catastrophic if operating temperatures are not well known.

4. Conclusions

Tantalum diboride was successfully densified by hot pressing at 1680 °C with addition of 10 vol% of $MoSi_2$; 5 vol% of sintering additive resulted in considerable level of porosity. The microstructure was homogeneous, with mean grain size around 3–4 μm; the matrix was not TaB_2 anymore, but a solid solution containing around 5 at% of Mo. Conversely $MoSi_2$ contained traces of tantalum and newly formed phases, such as Ta–Si and Ta–Mo–B compounds, SiC and a high amount of SiO_2. It is hypothesized that reciprocal cation diffusion occurred between TaB_2 and $MoSi_2$ giving rise to the $(Ta,Mo)B_2$ solid solution and Ta–Si compounds. Matter transfer mechanisms were enhanced by liquid phase constituted by Ta–Si–B–O.

The mechanical properties were generally good despite the presence of SiO_2 pockets all along the material. The silica softening was the reason for the high-temperature strength degradation, as it passed from about 630 MPa at room temperature to 200 MPa at 1200 °C and to 100 MPa at 1500 °C.

The oxidation of the composite was tested from 1200 to 1650 °C in a bottom-up furnace. TaB_2 remained apparently unaltered until 1600 °C and only a silica layer formed on the surface with maximum thickness of 9 μm. The bulk of the oxidized sample at 1600 °C resulted SiO_2-depleted, owing to its migration to the surface by capillary forces or its active oxidation and formation of gaseous SiO. At 1650 °C the material abruptly oxidized to Ta_2O_5 involving vigorous volatilization phenomena. Nanoindentation tests confirmed the different chemical composition just below the silica surface layer for a thickness of some hundreds μm.

This study pointed out that TaB_2 can be sintered at very low temperature with addition of $MoSi_2$ and it constitutes an excellent oxidation resistant material up to 1600 °C. The mechanical properties at room temperature are in the range of other UHTCs

based on ZrB_2 and HfB_2, but the removal of SiO_2 is necessary to preserve its properties at high temperature.

Acknowledgements

D. Dalle Fabbriche is acknowledged for hot pressing cycle and oxidation tests, G. Celotti for X-ray diffraction and V. Morandi for his assistance during TEM analysis.

References

1. Raju GB, Mukhopadhyay A, Biswas K, Basu B. Densification and high-temperature mechanical properties of hot pressed TiB_2–(0–10 wt.%)$MoSi_2$ composites. *Scr Mater* 2009;**61**:674–7.
2. Fahrenholtz WG, Hilmas GE, Talmy IG, Zaykoski JA. Refractory diborides of zirconium and hafnium. *J Am Ceram Soc* 2007;**90**:1347–64.
3. Guo SQ. Densification of ZrB_2-based composites and their mechanical and physical properties: a review. *J Eur Ceram Soc* 2009;**29**:995–1011.
4. Talmy IG, Zaykoski JA, Opeka MM, Dallek S. Oxidation of ZrB_2 ceramics modified with SiC and group IV–VI transition metal diborides. *Electrochem Soc Proc* 2001;**12**:144–58.
5. Speyer RF. Synthesis and processing of ultra-high temperature metal carbide and metal diboride nanocomposite materials. Technical Report 15 Apr 2008, FA9550-04-1-0140.
6. Peng F, Speyer RF. Oxidation resistance of fully dense ZrB_2 with SiC, TaB_2, and $TaSi_2$ additives. *J Am Ceram Soc* 2008;**91**:1489–94.
7. Peng F, Berta Y, Speyer RF. Effect of SiC, TaB_2 and $TaSi_2$ additives on the isothermal oxidation resistance of fully dense zirconium diboride. *J Mater Res* 2009;**24**:1855–67.
8. Zhang X, Hilmas GE, Fahrenholtz WG. Densification, mechanical properties and oxidation resistance of TaC–TaB_2 ceramics. *J Am Ceram Soc* 2008;**91**:4129–32.
9. Zhang X, Hilmas GE, Fahrenholtz WG. Synthesis, densification, and mechanical properties of TaB_2. *Mater Lett* 2008;**62**:4251–3.
10. Licheri R, Orrù R, Musa C, Cao G. Synthesis, densification and characterization of TaB_2–SiC composites. *Ceram Int* 2010;**36**:937–41.
11. Matsushita JI, Hwang GC, Shim KB. Oxidation behavior of tantalum boride ceramics. *Solid State Phenom* 2007;**124–126**:819–22.
12. Lee AJ, Baek SS, Kang ES, SM Y, Kim DK. Fabrication and oxidation behavior of reactively hot pressed TaB_2–SiC ceramics. *Rev Adv Mater Sci* 2011;**28**:21–5.
13. Kofstad P. Studies of the oxidation of tantalum at 1000–1300 °C. *J Less-Common Met* 1963;**5**:158–70.
14. Kofstad P. Low-pressure oxidation of tantalum at 1300–1800 °C. *J Less-Common Met* 1964;**7**:241–66.
15. Munz DG, Shannon JLJ, Bubsey RT. Fracture toughness calculation from maximum load in four point bend tests of chevron notch specimens. *Int J Fracture* 1980;**16**:R137–41.
16. Oliver WC, Pharr GM. An improved technique for determining hardness and elastic modulus using load and displacement sensing indentation experiments. *J Mater Res* 1992;**7**:1564–82.
17. Silvestroni L, Kleebe HJ, Lauterbach S, Müller M, Sciti D. Transmission electron microscopy on Zr- and Hf-borides with $MoSi_2$ addition: densification mechanisms. *J Mater Res* 2010;**25**:828–34.
18. Silvestroni L, Sciti D. Densification of ZrB2–TaSi2 and HfB2–TaSi2 ultra-high-temperature ceramic composites. *J Am Ceram Soc* 2011;**94**:1920–30.
19. Sciti D, Silvestroni L, Nygren M. Spark plasma sintering of ultra high temperature ceramics with decreasing amount of $MoSi_2$ as sintering aid. Zr- and Hf-borides. *J Eur Ceram Soc* 2008;**28**:1287–96.
20. Balbo A, Sciti D. Spark plasma sintering and hot pressing of ZrB_2–$MoSi_2$ ultra-high-temperature ceramics. *Mater Sci Eng A* 2008;**475**:108–12.
21. Sciti D, Silvestroni L, Bellosi A. Fabrication and properties of HfB_2–$MoSi_2$ composites produced by hot pressing and spark plasma sintering. *J Mater Res* 2006;**21**:1460–6.
22. Cutler RA. Engineering properties of borides. In: Schneider SJJ, editor. *Engineered materials handbook*. Metals Park, OH: ASM International; 1991. p. 787–803.
23. Jehn H, Olzi E. High temperature solid solubility limit and phase studies in the system tantalum-oxygen. *J Less-Common Met* 1972;**27**:297–309.
24. McColm J. Ceramic hardness. New York: Plenum Press; 1990.
25. Parthasarathy TA, Rapp RA, Opeka MM, Kerans RJ. A model for the oxidation of ZrB_2, HfB_2 and TiB_2. *Acta Mater* 2007;**55**:5999–6010.
26. Sciti D, Brach M, Bellosi A. Oxidation behaviour of a pressureless sintered ZrB_2–$MoSi_2$ composite. *J Mater Res* 2005;**20**:922–30.
27. Sciti D, Balbo A, Bellosi A. Oxidation behaviour of a pressureless sintered HfB_2–$MoSi_2$ composite. *J Eur Ceram Soc* 2009;**29**:1809–15.